

# Spatial and Seasonal Variations in C<sub>3</sub>H<sub>x</sub> Hydrocarbon Abundance in Titan's Stratosphere from Cassini CIRS Observations

Nicholas A Lombardo<sup>a,b,\*</sup>, Conor A Nixon<sup>a</sup>, Richard K Achterberg<sup>a,c</sup>, Antoine Jolly<sup>d</sup>, Keeyoon Sung<sup>e</sup>, Patrick G J Irwin<sup>f</sup>, F Michael Flasar<sup>a</sup>

<sup>a</sup>Planetary Systems Laboratory, Solar System Exploration Division, NASA Goddard Space Flight Center, 8800 Greenbelt Road, Greenbelt, MD, USA

<sup>b</sup>Center for Space Science and Technology, University of Maryland, Baltimore County, 1000 Hilltop Circle, Baltimore, MD, USA

<sup>c</sup>Department of Astronomy, University of Maryland College Park, College Park, MD, USA

<sup>d</sup>Laboratoire Interuniversitaire des Systemes Atmospheriques, Universite Paris Est, Creteil, France

<sup>e</sup>Jet Propulsion Laboratory, California Institute of Technology, Pasadena, CA, USA

<sup>f</sup>Department of Atmospheric, Oceanic, and Planetary Physics, Camden College, University of Oxford, Oxford, UK

---

## Abstract

Of the C<sub>3</sub>H<sub>x</sub> hydrocarbons, propane (C<sub>3</sub>H<sub>8</sub>) and propyne (methylacetylene, CH<sub>3</sub>C<sub>2</sub>H) were first detected in Titan's atmosphere during the Voyager 1 flyby in 1980. Propene (propylene, C<sub>3</sub>H<sub>6</sub>) was first detected in 2013 with data from the Composite InfraRed Spectrometer (CIRS) instrument on Cassini. We present the first measured abundance profiles of propene on Titan from radiative transfer modeling, and compare our measurements to predictions derived from several photochemical models. Near the equator, propene is observed to have a peak abundance of 10 ppbv at a pressure of 0.2 mbar. Several photochemical models predict the amount at this pressure to be in the range 0.3 - 1 ppbv and also show a local minimum near 0.2 mbar which we do not see in our measurements. We also see that propene follows a different latitudinal trend than the other C<sub>3</sub> molecules. While propane and propyne concentrate near the winter pole, transported via a global convective cell, propene is most abundant above the equator. We retrieve vertical abundances profiles between 125 km and 375 km for these gases for latitude averages between 60°S to 20°S, 20°S to 20°N, and 20°N to 60°N over two time periods, 2004 through 2009 representing Titan's atmosphere before the 2009 equinox, and 2012 through 2015 representing time after the equinox. Additionally, using newly corrected line data, we determined an updated upper limit for allene (propadiene, CH<sub>2</sub>CCH<sub>2</sub>), the isomer of propyne). The measurements we present will further constrain photochemical models, by refining reaction rates and the transport of these gases throughout Titan's atmosphere.

---

\*Corresponding author: Nicholas Lombardo, nicholas.lombardo@nasa.gov

## 30 1. Introduction

31 Titan, the largest moon of Saturn, is thought to have many similarities to the Archean Earth, including  
32 an atmosphere dominated by  $N_2$ , significant quantities of  $CH_4$ . The surface mixing ratio is 5% measured  
33 by the Huygens GCMS Niemann et al. (2010), and decreasing with altitude into the stratosphere where  
34 it remains constant with altitude at 1-1.5% as measured in Lellouch et al. (2014) on Titan. Global haze  
35 layers which continually shroud Titan and may have occurred intermittently on Earth. While factors like  
36 temperature, sources of atmospheric  $CH_4$ , and minor atmospheric constituents vary between the two bodies,  
37 Titan remains a good analog for studying the atmosphere of the Archean Earth (Izon et al., 2017), (Arney  
38 et al., 2016).

39 The global haze on Titan is produced through photolysis of  $CH_4$  as Saturn Magnetospheric Electrons  
40 and solar UV photons bombard the upper atmosphere. The products of this process -highly reactive  $CH_3^-$ ,  
41  $H^+$ , and  $N^+$  ions, among others- may then react to form  $C_2H_6$ ,  $C_2H_4$ , and other molecules. As this complex  
42 process continues, larger hydrocarbons ( $C_xH_y$ ) and nitriles ( $C_xH_y(CN)_z$ ) react further to give rise to the  
43 'photochemical zoo' of molecules present in Titan's atmosphere (Yung et al., 1984; Wilson and Atreya, 2004).

44 Titan's  $26.7^\circ$  obliquity, comparable to the Earth's  $23.5^\circ$  obliquity, causes variations in the insolation of  
45 the moon over the course of a Titan year (about 29.5 Earth years). The resulting seasonal variations in  
46 the physical state of the atmosphere have been observed and modeled in Caldwell et al. (1992), Lebonnois  
47 et al. (2001), Jennings et al. (2012), Teanby et al. (2012), Vinatier et al. (2015), and Coustenis et al. (2016),  
48 among others, see review by (Horst, 2017). Noteworthy is the existence of a global circulation cell, which  
49 transports warm gases in the summer hemisphere towards the winter pole, where they subside lower into the  
50 stratosphere. This downward advection causes adiabatic warming in the winter stratosphere and entrains  
51 short-lived gases produced in the upper stratosphere, increasing their abundance lower in the atmosphere.  
52 As northern winter evolved to northern spring, this single circulation cell transformed into two circulation  
53 cells, upwelling near the equator and downwelling at both poles, as predicted in Hourdin et al. (2004)  
54 and observed in Vinatier et al. (2015). For additional explanation of Titan's atmospheric dynamics and  
55 chemistry, the reader is directed to (Müller-Woodarg et al., 2014) and (Brown et al., 2010).

56 Regarding the  $C_3$  hydrocarbons, propane ( $C_3H_8$ ) and propyne ( $C_3H_4$ ) were initially detected in Titan's  
57 atmosphere after the 1980 Voyager 1 flyby (Hanel et al., 1981) through spectra acquired by the IRIS instru-  
58 ment. Abundances for propyne were first estimated by (Maguire et al., 1981) by comparing the strength of  
59 the  $633\text{ cm}^{-1}$  Q-branch of propyne to the  $721\text{ cm}^{-1}$  Q-branch of acetylene (also ethyne,  $C_2H_2$ ), and esti-  
60 mated to be on the order of  $3 \times 10^{-8}$ . Propane was modeled in the same paper using a synthetic spectrum

61 constructed for its  $\nu_{21}$  band, and a disk averaged value of  $2 \times 10^{-5}$  was reported. These values were updated  
62 by Coustenis et al. (1989) to  $4.4^{+1.7}_{-2.1} \times 10^{-9}$  for propyne and  $(7 \pm 4) \times 10^{-7}$  for propane. Further weak bands  
63 of propane were detected by the Composite InfraRed Spectrometer (CIRS) aboard Cassini (Nixon et al.,  
64 2009). Over three decades later, CIRS spectra were used to make the first detection of  $C_3H_6$  (Nixon et al.,  
65 2013), however an exact abundance could not be retrieved from modeling the spectra due to the lack of a  
66 spectral line list, although an abundance estimate was made by comparing the intensities of propene and  
67 propane lines, discussed more in Section 4.2.

68 Recent analyses have shown the abundance of propyne to vary strongly with season and latitude. Vinatier  
69 et al. (2015), using limb viewing observations, showed the vertical gradient of  $C_3H_4$  increases dramatically  
70 over the mid northern latitudes as northern winter moves into northern spring and the polar vortex responds  
71 to the changing amount of sunlight. Coustenis et al. (2018), using nadir observations to probe abundance  
72 in a narrow altitude range in the low stratosphere, show a similar trend at latitudes closer to the pole,  
73 between  $60^\circ$  and  $90^\circ$  either side of the equator. In the same studies, propane was shown to have a more  
74 constant abundance in latitude and time, remaining constant within error bars near  $1 \times 10^{-6}$  throughout the  
75 stratosphere, with the exception near the winter pole, where it increases with altitude.

76 Two  $C_3$  hydrocarbons have yet to be firmly detected on Titan, allene ( $CH_2CCH_2$ , isomer of propyne)  
77 and cyclopropane ( $CH_2CH_2CH_2$ , isomer of propene). There was a tentative detection of allene by Roe et al.  
78 (2011), however an accurate linelist was not available at the time of the study, thus the authors were not  
79 able to model the potential allene feature and confirm its detection. In this paper, we discuss members of  
80 the  $C_3H_x$  series known to be present in Titan's atmosphere- propane ( $C_3H_8$ ), propene ( $C_3H_6$ ), and propyne  
81 ( $CH_3C_2H$ ). We also searched for allene and provide an new upper limit for allene in regions close to the  
82 equator. This work was enabled by the creation of a propene pseudo-line list for Titan (Sung et al., 2018)  
83 and an updated line list for allene (see Section 2.2).

84 We use spectra collected by the CIRS instrument to determine the abundance of propene in Titan's strato-  
85 sphere. We show latitudinal and seasonal variation in the distribution of propene, propane and propyne.  
86 The large number of CIRS observations used allows us to vertically resolve the profile of each gas. We  
87 compare the values determined to those predicted by photochemical models of Hébrard et al. (2013), Li  
88 et al. (2015), Loison et al. (2015), and Krasnopolsky (2014).

## 89 2. Methods

### 90 2.1. Dataset

91 CIRS is a Fourier Transform infrared spectrometer, with three focal planes spanning the  $10\text{ cm}^{-1}$  -  $1500$   
92  $\text{cm}^{-1}$  spectral region (Jennings et al., 2017). We use spectra acquired by Focal Plane 3 (FP3,  $580\text{ cm}^{-1}$ -  
93  $1100\text{ cm}^{-1}$ ) and Focal Plane 4 (FP4,  $1050\text{ cm}^{-1}$ - $1500\text{ cm}^{-1}$ ), two parallel arrays of 10 detectors each. Limb  
94 observations were performed at a spectral resolution of  $0.5\text{ cm}^{-1}$  at distances between  $10^5\text{ km}$  and  $2\times 10^5$   
95  $\text{km}$  from Titan, during which time each focal plane was positioned normal to Titan’s surface, such that each  
96 detector sampled a different altitude. The arrays were centered at  $125\text{ km}$  for between one and two hours  
97 and were then moved away from Titan’s surface to stare at a central altitude of  $350\text{ km}$  for a similar amount  
98 of time. The footprint of each detector (the vertical resolution) on Titan’s atmosphere varied between  $27$   
99  $\text{km}$  and  $54\text{ km}$  depending on the distance to the moon. The size of the footprint was comparable to Titan’s  
100 atmospheric scale height, and thus allows us to vertically resolve physical characteristics of the atmosphere.

101 The  $\text{C}_3\text{H}_6\ \nu_{19}$  band detected in Nixon et al. (2013) at  $912.67\text{ cm}^{-1}$  sits between several  $\text{C}_2\text{H}_4$  emissions,  
102 and on top of a broad  $\text{C}_3\text{H}_8$  band. To increase S/N to the point where we can model this feature, we chose  
103 to combine data from several flybys of Titan that are comparable in temperature. This results in averaging  
104 data from between three and seven flybys (or between 187 and 728 spectra) per time-latitude bin on Titan.  
105 We use two time periods - the pre equinox time from 2005 through 2008 (just before the northern vernal  
106 equinox of August 2009) and the post equinox time 2012 through 2015. During the time just after the  
107 northern vernal equinox, Cassini was in a very low inclination orbit relative to Saturn. Limb observations  
108 on Titan were focused on the polar regions, as Cassini was able to view these regions of the atmosphere  
109 continuously during a Titan flyby. We therefore do not include data from just after the equinox, as no limb  
110 data exists for the latitude regions we model in this work. In each time span, we combine observations  
111 representative of three latitude regions - northern, equatorial, and southern.

112 In our averages, we include data from  $20^\circ$  to  $60^\circ$  for both hemispheres, and within  $20^\circ$  of the equator. The  
113 former two bins represent the midlatitudes, and the third bin represent the equatorial atmosphere. While  
114 the latitude boundaries for observations we include are the same before and after equinox, the physical  
115 distribution of included observations varies. As an example, in the pre-equinox time, the northern bin  
116 contains observations from  $24^\circ\text{N}$  through  $54^\circ$ , whereas post-equinox we have observations only between  
117  $25^\circ\text{N}$  and  $48^\circ\text{N}$ . The distribution of observations used is shown in Fig. 1 as black dots. The boundaries for  
118 each time-latitudinal bin are drawn as black boxes enclosing observations. We exclude observation centered  
119 at latitudes closer than  $60^\circ$  to either pole because temperature begins to vary strongly with latitude in these

120 regions. Including these spectra in our averages would make the resultant spectra very difficult to model  
121 and obscure details of finer latitudinal variations in the retrieved profiles.

## 122 2.2. Spectral Line Data

123 Molecular line lists used were derived from the HITRAN (Gordon et al., 2017) and GEISA (Jacquinet-  
124 Husson et al., 2016) databases. The exceptions are propane (Sung et al., 2013), propene (Sung et al., 2018),  
125 propyne (previously used in in Coustenis et al. (2007)), diacetylene (Jolly et al., 2010), and allene, discussed  
126 below.

### 127 2.2.1. Updated Allene Linedata

128 No allene line lists are present either in HITRAN nor in GEISA but Coustenis et al. (1993) previously  
129 investigated the detectability of allene in Titan’s atmosphere using spectroscopic parameters by Chazelas  
130 et al. (1985) for the  $\nu_{10}$  band centered at  $845\text{ cm}^{-1}$ . Line intensities were obtained from band intensity  
131 measurements by Koga et al. (1979). They concluded that the non-detection of allene implied an abundance  
132 below 5 ppbv.

133 In addition to this existing spectroscopic data, we include parameters obtained by high resolution studies  
134 (Hegeland et al., 1993) that address the existence of hot bands. The hot band contribution is necessary at  
135 room temperature to allow comparisons between these calculated line lists with observed room temperature  
136 spectra. Calculations were compared and validated against room and high temperature spectra taken at  
137  $0.08\text{ cm}^{-1}$  resolution in the  $\nu_{10}/\nu_9$  wavenumber range (Es-sebbar et al., 2014). Comparisons between the  
138 calculated linelists and observed spectra are given in Jolly et al. (2015).

## 139 2.3. Radiative Transfer Modeling

140 Spectral fitting was done using the NEMESIS atmospheric modeling code (Irwin et al., 2008). NEMESIS  
141 operates on the method of optimal estimation, which involves the computation of a forward model and a  
142 retrieval process. The forward model was calculated using the correlated-k method of Lacis and Oinas  
143 (1991), and includes a Hamming apodization of Full Width at Half Maximum of  $0.475\text{ cm}^{-1}$  to recreate  
144 the instrument line shape. The retrieval process varies *a priori* profiles of chosen physical parameters to  
145 optimize the spectral fits. This is done by minimizing a cost-function which includes the deviation of the  
146 retrieved profile from the *a priori* estimate, and the quality of fit to the spectra (similar to a  $\chi^2$  goodness  
147 of fit test). NEMESIS has been extensively used to determine atmospheric abundances in the outer solar  
148 system using IR spectra, and application to Titan is described in Teanby et al. (2007), Teanby et al. (2009b),  
149 and Cottini et al. (2012).

150 Spectral modeling proceeded in two steps: stratospheric temperatures during observations were ex-  
 151 tracted, then the abundances of trace gases were retrieved. First, the 1275  $\text{cm}^{-1}$  - 1325  $\text{cm}^{-1}$  region of  
 152 the  $\nu_4$  band of methane was modeled to extract the stratospheric temperature profile. While we did not  
 153 model the entire  $\nu_4$  band that extends from 1250  $\text{cm}^{-1}$  - 1350  $\text{cm}^{-1}$ , the region of the spectrum we modeled  
 154 contains sufficient information to retrieve the temperatures in the altitude regions needed for modeling the  
 155 trace gases. Temperature measurements proceeded by assuming a methane abundance of  $1.41 \times 10^{-2}$  above  
 156 140 km, consistent with previous measurements and models (Lellouch et al., 2014), (Wilson and Atreya,  
 157 2004)) and an abundance below 140 km derived from measurements by the Huygens descent profile (Nie-  
 158 mann et al., 2010). The initial temperature profile was derived from the HASI temperature (Fulchignoni  
 159 et al., 2005) profile, and a non-gray aerosol haze was also allowed to vary. This retrieved temperature was  
 160 then fixed while gases in the FP3 spectral region were allowed to vary. In the 900  $\text{cm}^{-1}$  - 930  $\text{cm}^{-1}$  region,  
 161 the Q branch of the  $\nu_{21}$  band of propane at 922  $\text{cm}^{-1}$ , the  $\nu_{19}$  propene band at 912.5  $\text{cm}^{-1}$ , and  $\nu_7$  lines of  
 162 ethylene at 915.5  $\text{cm}^{-1}$  and 922.5  $\text{cm}^{-1}$  were modeled. In the 620  $\text{cm}^{-1}$  - 640  $\text{cm}^{-1}$  region, the propyne  $\nu_9$   
 163 band at 633  $\text{cm}^{-1}$  and diacetylene  $\nu_8$  band at 628  $\text{cm}^{-1}$  were modeled.

164 The *a priori* volume mixing ratios (VMRs) used were constant over our range of sensitive altitudes  
 165 above 100 km and set to values comparable to those reported in previous literature including Coustenis  
 166 et al. (2007), Vinatier et al. (2007), Coustenis et al. (2010), and Vinatier et al. (2015), and represent 'rough  
 167 guesses' for the abundance of each molecule in both time spans. Though some molecules have been shown  
 168 to have vertical gradient that changes with time, we chose to use a constant profile above saturation that  
 169 is the same for both time spans as to not influence the results of our comparisons across latitude and time.  
 170 The *a priori* value for propene is comparable to predictions from Hébrard et al. (2013), Nixon et al. (2013),  
 171 Li et al. (2015), and Dobrijevic et al. (2016).

Gas	<i>a priori</i> VMR
$\text{C}_2\text{H}_4$	$(1.1 \pm 0.2) \times 10^{-7}$
$\text{C}_3\text{H}_8$	$(1 \pm 0.5) \times 10^{-6}$
$\text{C}_3\text{H}_6$	$(3 \pm 1.5) \times 10^{-9}$
$\text{CH}_3\text{C}_2\text{H}$	$(1 \pm 0.4) \times 10^{-8}$
$\text{C}_4\text{H}_2$	$(5 \pm 2.5) \times 10^{-9}$

### 172 3. Results

173 Example spectra from the altitude bins used in the pre-equinox southern temperature retrieval are shown  
 174 in Fig 2. Errors on the radiance were expanded to account for systematic uncertainties and prevent over-  
 175 constraining the model. Normalized contribution functions - also called the inversion kernel are the rate

176 of change of radiance with respect to abundance. Altitudes with higher values 'contribute' more to the  
177 calculated spectrum, and thus are the altitudes where the data give the most information - see Fig. 3.  
178 Retrieved temperature profiles for the pre-equinox time span and the post-equinox time span are shown in  
179 Fig. 4. We see variation in the stratospheric temperature and the shape and altitude of the stratopause as  
180 described in Flasar and Achterberg (2009). While the stratopause increases in altitude towards the north  
181 winter pole, we do not see the full extent of the stratopause, since our data is only sensitive to an altitude  
182 of 0.02 mbar. Contribution functions similar to Fig. 3 are shown in Fig. 5 for the propene retrieval. Figs.  
183 6 and 7 show spectral fits for the pre-equinox southern bin, similar to those shown for temperature. The  
184 retrieved profiles of  $C_3H_4$ ,  $C_3H_6$ ,  $C_3H_8$  are given in Fig. 8 and Fig. 9.

185 The  $C_3H_8$  profile shows a peak stratospheric abundance at 0.5 mbar in the north during late winter,  
186 with the profile flattening out to a more vertically constant profile in the equatorial and southern bins. The  
187 post-equinox profiles show the peak altitude decreasing slightly in the north, and a similar peak at 0.7 mbar  
188 forming around the equator during early northern spring.

189  $C_3H_6$  does not follow the same trend as other  $C_3$  hydrocarbons, the maximum abundance of the gas in  
190 both time seasons is above 1 mbar near the equator. This differs from the general trend of the other  $C_3$   
191 hydrocarbons and trace gases, which tend to increase above the mid to high winter latitudes.

192  $CH_3C_2H$  shows a nearly constant abundance within error bars in the northern pre-equinox bin, becoming  
193 more variable and decreasing in abundance as the latitude moves away from the winter pole. The  $CH_3C_2H$   
194 abundance profiles for the post-equinox time span are comparable across latitudes. There appears to be some  
195 small but systematic error of the  $CH_3C_2H$  spectral fit that may require re-evaluation of the methylacetylene  
196 line list. This misfit is also seen in Fig. 10 of Vinatier et al. (2007) and Fig. 12 of Coustenis et al. (2007).

## 197 4. Discussion

### 198 4.1. Propane

199 In the pre-equinox period, equatorial and southern propane increases with altitude from  $5 \times 10^{-7}$  at  
200 10 mbar to  $1 \times 10^{-6}$  at 0.01 mbar. In the north (during winter at the time), the abundance achieves  
201 a maximum abundance of  $1 \times 10^{-6}$  at 0.3 mbar before it begins to decrease with altitude, returning the  
202 a similar abundance as in the southern and equatorial regions. In the post-equinox period, the propane  
203 distribution remains largely unchanged within errorbars. The south shows the abundance around 1 mbar  
204 decrease from  $1 \times 10^{-6}$  to  $8 \times 10^{-7}$ , just outside of the errorbars on the retrieval.

205 We are able to compare to Vinatier et al. (2007), who measure abundance from the first flyby of Titan  
206 by Cassini, Tb on 13 December 2004, at 15 °S. They show propane increasing monotonically from  $4 \times 10^{-7}$

207 at 4 mbar to  $1 \times 10^{-6}$  at 0.01 mbar, which has a slightly greater slope than our pre-equinox values. In  
 208 comparison, Bampasidis et al. (2012) probe the lower stratosphere using nadir observations between 2006  
 209 and 2012, they show propane generally at an southern and equatorial abundance of  $5 \times 10^{-7}$  between 2006  
 210 and 2009, in agreement with our results. At  $50^\circ\text{N}$ , they retrieve an abundance near  $2 \times 10^{-6}$ , which is  
 211 slightly higher than our values at the lowest altitudes, but agree with our limb sounding around 3 mbar.  
 212 Vinatier et al. (2015) perform another analysis of chemical abundance during the northern spring, between  
 213 2009 and 2013. At  $46^\circ\text{N}$  in 2012, they show propane at  $4 \times 10^{-7}$  at 5 mbar increasing to  $1 \times 10^{-6}$  at 0.03  
 214 mbar. Because their analysis was done on a single observation, the errorbars presented are large, so it is  
 215 hard to compare variations in the vertical profile with our results, however they do seem compatible.

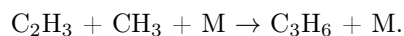
#### 216 4.2. Propyne

217 Propyne shows stronger seasonal variation than propane. In the pre-equinox period, our results show  
 218 propyne having a weak vertical gradient from  $8 \times 10^{-9}$  at 8 mbar to just under  $2 \times 10^{-8}$  at 0.01 mbar in the  
 219 south. The vertical gradient decreases near the equator, and becomes nearly vertical in the north, indicative  
 220 of the effect of downward advection within the winter polar vortex on the abundance profiles of trace gases..  
 221 In the post-equinox period, the propyne profile become similar across all latitudes, increasing from  $1 \times 10^{-8}$   
 222 at 8 mbar to  $2 \times 10^{-8}$  at 0.01 mbar. Bampasidis et al. (2012) report similar values to ours for the 2006-2009  
 223 period for  $50^\circ\text{N}$ ,  $0^\circ\text{N}$ , and  $50^\circ\text{S}$ . Vinatier et al. (2007) show a steeper vertical profile at  $15^\circ\text{S}$  than our results  
 224 indicate. Their modeled profile begins at a slightly lower abundance at 1 mbar and is in agreement with our  
 225 results at higher altitudes. This could be explained by our larger dataset including observations later in the  
 226 season and at slightly higher latitudes, where we would expect to see more propyne at lower altitudes.

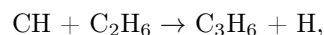
#### 227 4.3. Propene

228 Photochemical models have included  $\text{C}_3\text{H}_6$  beginning after the Voyager flyby (Yung et al., 1984). Since  
 229 the start of the Cassini mission, several new models have also incorporated the molecule (Wilson and Atreya,  
 230 2004; Hébrard et al., 2013; ?; Krasnopolsky, 2014; Li et al., 2015; Loison et al., 2015; Dobrijevic et al., 2016).

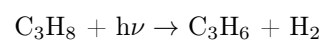
231 Yung et al. (1984) propose the main source of propene in Titan's stratosphere ( $<300$  km) is from



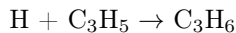
232 Li et al. (2015) follow with additional production pathways



233 dominating the region between 600 km and 1000 km, where CH molecules are plentiful and



234 dominating the region between 300 km and 600 km, where the pressure is not great enough for a termolecular  
235 reaction and CH is scarce. Alternatively, Hébrard et al. (2013) include



236 as the dominating production reactions at mid to high altitudes.

237 The first detection of  $\text{C}_3\text{H}_6$  in Titan's atmosphere was made with the INMS instrument by Magee et al.  
238 (2009). However, because mass spectrometers can generally not differentiate between isomers, it is unknown  
239 whether this detection is of propene or cyclopropane. The first definitive detection of propene was made  
240 by Nixon et al. (2013) using an average of CIRS spectra between  $30^\circ\text{S}$  and  $10^\circ\text{N}$  from 1 July 2004 through  
241 1 July 2010, similar to our  $20^\circ\text{S}$ - $20^\circ\text{N}$  pre-equinox bin. However, a spectral line list for propene did not  
242 exist at the time, so the gas could not be included in their radiative transfer calculations. Instead, estimates  
243 of abundance were made by comparing the relative intensities of the propane and propene lines, and they  
244 claimed a  $3\text{-}\sigma$  abundance of  $(2.0\text{-}4.6)\times 10^{-9}$  between 100 and 200 km.

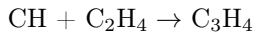
245 In Fig. 10, we compare the predicted propene profiles to the abundance we determined for the pre-equinox  
246 time span, centered on the equator. Of the models compared, Loison et al. (2015) shows the best agreement.  
247 The abundance below 6 mbar is within the errorbars of our measured values. Above that, our measurements  
248 are within the 90th percentile of modeled profiles (90th percentile being the region which encloses 90% of  
249 modeled profiles.) In all other cases, the predictions have a peak abundance at or below 1 mbar, ranging  
250 from 1 to 6 ppbv. Our profiles display a peak abundance of 10 ppbv at 0.1 mbar, higher in abundance and  
251 altitude than all of the compared profiles. The profiles from Li et al. (2015) and Krasnopolsky (2014) show  
252 good agreement in abundance below 1 mbar, but also display an inversion above 0.2 mbar that we do not  
253 see in our measurements. We also retrieve about twice as much propene compared to the values inferred  
254 from relative line strengths in Nixon et al. (2013).

255 A modified version of the Loison et al. (2015) model was used as the Dobrijevic et al. (2016) model.  
256 Since the two models have different predicted profiles for propene, we can look at the differences between  
257 the two models in attempt to isolate the factors that caused the abundance of propene to change. Dobrijevic  
258 et al. (2016) list the changes from Loison et al. (2015) as: limiting the modeled hydrocarbons at  $\text{C}_4$  species,  
259 excluding high mass nitriles, reducing the number of isomers included, and not considering reactions with  
260 'very small fluxes'. The authors checked the effects of these changes on species included in the model,  
261 and while no major change was reported for significant molecules, we do see that the changes applied in  
262 Dobrijevic et al. (2016) decrease the predicted abundance of propene and worsen the agreement between the  
263 Loison et al. (2015) and our measurements. Due to the large number of reactions included in both models,

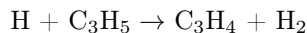
264 we are unable to say which of these changes has the greatest effect on the modeled abundance of propene.

#### 265 4.4. Allene

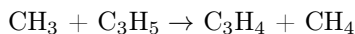
266 The isomer of propyne,  $\text{CH}_2\text{CCH}_2$  or allene, is also theorized to be produced in Titan's atmosphere  
267 (Yung et al., 1984; Li et al., 2015). Production pathways for allene (and propyne) include



268 above 600 km, with



269 and



270 dominating throughout the rest of the atmosphere.

271 The only potential detection of allene on Titan was made in Roe et al. (2011), however since the line  
272 list used in the authors' analysis was in significant disagreement with the potential observed allene lines this  
273 remains only a tentative detection. Other analyses of Titan's atmosphere to search for allene have resulted in  
274 many upper limits. Coustenis et al. (2003) claimed a  $3\text{-}\sigma$  upper limit of 2 ppbv, derived from disk averaged  
275 spectra from the Infrared Space Observatory (ISO). Nixon et al. (2010) estimate a  $3\text{-}\sigma$  upper limit of 0.3  
276 ppbv at  $25^\circ\text{ N}$  at 107 km, and 1.6 ppbv at  $76^\circ\text{ N}$ , 224 km, using a method described in their paper. We  
277 update these upper limits using a corrected line list produced by us and included in our radiative transfer  
278 calculations.

279 The spectrum used in the model is an average of nadir observations between  $30^\circ\text{S}$  and  $30^\circ\text{N}$ , from 2004-  
280 2015. Nadir observations were used to take advantage of the lower noise compared to limb viewing, however  
281 the abundance of allene is likely to be very low at the altitudes that nadir observations are sensitive to. Fig.  
282 11 shows the best fit spectrum overlayed on the observed spectrum. The contributions of allene are visible  
283 as spikes in the dotted-line residual.

284 We perform a  $\Delta\chi^2$  analysis similar to that described in Teanby et al. (2007) and Nixon et al. (2010)  
285 and estimate a  $2\text{-}\sigma$  upper limit of 1 ppbv at 150 km within  $30^\circ$  North and South of the equator. A retrieval  
286 was performed between 830 and  $880\text{ cm}^{-1}$  including ethane and propane spectral data, as for the previously  
287 described retrievals. The  $\chi^2$  value for this retrieval was considered  $\chi_0^2$ . The best-fit abundances of ethane  
288 and propane were then held constant and varying amounts of allene were added to the atmosphere model.  
289 A forward model was run at each allene abundance to calculate a modified chi-squared value ( $\chi_m$ ), the  $\Delta\chi^2$   
290 value was calculated to be  $\chi_m^2 - \chi_0^2$ . We plot the values of  $\Delta\chi^2$  as a function of added allene in Fig. 12.  
291 Where the  $\Delta\chi^2$  achieves a minimum value, we claim an upper limit with a confidence of  $(\Delta\chi^2)^{1/2}$ . The

292 results are shown in Fig. 11 and Fig. 12. A major challenge to modeling this allene band is the overlap  
293 of the band with the band of ethane and the band of propane. The ethane band is very bright, as seen in  
294 Fig. 11. Therefore, relatively small discrepancies in the modeling and linelist of ethane propagate heavily  
295 through to measuring allene. The propane band also present in the region we modeled is very dim and  
296 broad, further increasing the difficulty of measuring allene in this region, since it contributes mostly to the  
297 continuum in this small spectral window.

## 298 5. Conclusion

299 In this work, we have determined the first abundance profiles of propene in Titan’s atmosphere, enabling  
300 us to compare the mixing ratio and spatial distribution of this gas with other trace gases, as well as compare  
301 to predictions from existing photochemical models. In brief, we’ve shown:

- 302 1. propene is present in Titan’s atmosphere at a mixing ratio between 4 and 10 ppbv in the stratosphere
- 303 2. the abundance of propene near the equator is consistent with predictions from the Loison et al. (2015)  
304 model, but other predictions show a local inversion centered around 0.1 mbar, and a generally lower  
305 abundance
- 306 3. contrary to other trace gases, propene does not show a poleward enhancement in the winter hemisphere  
307 equatorward of 60°. Instead, propene shows an increased abundance above the equator relative to  
308 either pole.

309 The results of our analysis will be useful in refining models of Titan’s atmospheric chemistry and dynamics  
310 as discrepancies between observations and predictions show that current photochemical models do not  
311 accurately predict the production and destruction rates of the molecule. Propene’s unique spatial trend  
312 will make it a useful constraint in global circulation and transport models, as it may be a good tracer for  
313 horizontal transport. Additionally, the polymerization of propene and other  $\pi$ -bond molecules may lead to  
314 the formation of aerosols (Teanby et al., 2009a; Trainer et al., 2013)

315 Our updated upper limit for allene, calculated using the corrected linelist will also help to constrain  
316 theoretical production rates of the currently undetected gas.

## 317 6. Acknowledgments

318 N.A.L., C.A.N., R.K.A., and F.M.F. were supported by the NASA Cassini Project for the research work  
319 reported in this paper. Part of the research was carried out at the Jet Propulsion Laboratory, California  
320 Institute of Technology, under a contract with the National Aeronautics and Space Administration.

## 321 7. References

- 322 Achterberg, R. K., Gierasch, P., Contrath, B., Flasar, F., Jennings, D. E., Nixon, C. A., Nov. 2014. Post-equinox Variations of  
323 Titan's Mid-stratospheric Temperatures from Cassini/CIRS Observations. In: AAS/Division for Planetary Sciences Meeting  
324 Abstracts. Vol. 46 of AAS/Division for Planetary Sciences Meeting Abstracts. p. 102.07.
- 325 Arney, G., Domagal-Goldman, S. D., Meadows, V. S., Wolf, E. T., Schwieterman, E., Charnay, B., Claire, M., Hebrard, E.,  
326 Trainer, M. G., 2016. The pale orange dot: The spectrum and habitability of hazy Archean Earth. *Astrobiology* 16, 873 –  
327 899.
- 328 Bampasidis, G., Coustenis, A., Achterberg, R. K., Vinatier, S., Lavvas, P., Nixon, C. A., Jennings, D. E., Teanby, N. A.,  
329 Flasar, F. M., Carlson, R. C., Moussas, X., Preka-Papadema, P., Romani, P. N., Guandique, E. A., Stamogiorgos, S., 2012.  
330 Thermal and chemical structure variations in Titan's stratosphere during the Cassini mission. *The Astrophysical Journal*  
331 760 (2), 144–152.
- 332 Brown, R., Lebreton, J. P., Waite, J. (Eds.), 2010. *Titan from Cassini Huygens*. Springer.
- 333 Caldwell, J., Cunningham, C. C., Anthony, D., White, H. P., Groth, E. J., Hasan, H., Noll, K., Smith, P. H., Tomasko, M. G.,  
334 Weaver, H. A., 1992. Titan: Evidence for seasonal change a comparison of Hubble Space Telescope and Voyager images.  
335 *Icarus* 96, 1–9.
- 336 Chazelas, J., Pliva, J., Valentin, A., Henry, L., 1985. Analysis of the  $\nu_9/\nu_{10}$  band system of allene. *Journal of Molecular*  
337 *Spectroscopy* 110, 326–338.
- 338 Cottini, V., Nixon, C., Jennings, D., Anderson, C., Gorius, N., Bjoraker, G., Coustenis, A., Teanby, N., Achterberg, R.,  
339 Bézard, B., de Kok, R., Lellouch, E., Irwin, P., Flasar, F., Bampasidis, G., 2012. Water vapor in Titan's stratosphere  
340 from Cassini CIRS far-infrared spectra. *Icarus* 220, 855–862.
- 341 Coustenis, A., Achterberg, R. K., Conrath, B. J., Jennings, D. E., Marten, A., Gautier, D., Nixon, C. A., Flasar, F. M., Teanby,  
342 N. A., Bézard, B., Samuelson, R. E., Carlson, R. C., Lellouch, E., Bjoraker, G. L., Romani, P. N., Taylor, F. W., Irwin,  
343 P. G., Fouchet, T., Hubert, A., Orton, G. S., Kunde, V. G., Vinatier, S., Mondellini, J., Abbas, M. M., Courtin, R., 2007.  
344 The composition of Titan's stratosphere from Cassini/CIRS mid-infrared spectra. *Icarus* 189, 35–62.
- 345 Coustenis, A., Bézard, B., Gautier, D., 1989. Titan's atmosphere from Voyager infrared observations, i. the gas composition of  
346 Titan's equatorial region. *Icarus* 80, 54–76.
- 347 Coustenis, A., Encrenaz, T., Bézard, B., Bjoraker, G., Graner, G., Dang-Nhu, M., Arié, E., 1993. Modelling Titan's thermal  
348 infrared spectrum for high resolution space observations. *Icarus* 102, 240–260.
- 349 Coustenis, A., Jennings, D. E., Achterberg, R. K., Bampasidis, G., Lavvas, P., Nixon, C. A., Teanby, N. A., Anderson, C. M.,  
350 Cottini, V., Flasar, F. M., 2016. Titan's temporal evolution in stratospheric trace gases near the poles. *Icarus* 270, 409–420.
- 351 Coustenis, A., Jennings, D. E., Achterberg, R. K., Bampasidis, G., Nixon, C. A., Lavvas, P., Cottini, V., Flasar, F. M., 2018.  
352 Seasonal evolution of Titan's stratosphere near the poles. *The Astrophysical Journal* 854, L30–L37.
- 353 Coustenis, A., Jennings, D. E., Nixon, C. A., Achterberg, R. K., Lavvas, P., Sinatier, S., Teanby, N. A., Bjoraker, G. L.,  
354 Carlson, R. C., Piani, L., Bampasidis, G., Flasar, F. M., Romani, P. N., 2010. Titan's trace gas composition from CIRS at  
355 the end of the Cassini-Huygens prime mission. *Icarus* 207, 461 – 476.
- 356 Coustenis, A., Salama, A., Schulz, Ott, S., Lellouch, E., Encrenaz, T., Gautier, D., Feuchtgruber, H., 2003. Titan's atmosphere  
357 from ISO mid-infrared spectroscopy. *Icarus* 161, 383–403.
- 358 Dobrijevic, M., Loison, J., Hickson, K., Gronoff, G., 2016. 1d-coupled photochemical model of neutrals, cations and anions in  
359 the atmosphere of Titan. *Icarus* 268, 313–339.
- 360 Es-sebbar, E., Jolly, A., Benilan, Y., Farooq, A., 2014. Quantitative mid-infrared spectra of allene and propyne from room to  
361 high temperatures. *Journal of Molecular Spectroscopy* 305, 10–16.
- 362 Flasar, F. M., Achterberg, R. K., 2009. The structure and dynamics of Titan's middle atmosphere. *Philosophical Transactions*  
363 *of the Royal Society A* 367, 649–664.
- 364 Fulchignoni, M., Ferri, F., Angrilli, F., Ball, A. J., Bar-Nun, A., Barucci, M. A., Bettanini, C., Bianchini, G., Borucki,  
365 W., Colombatti, G., Coradini, M., Coustenis, A., Debei, S., Falkner, P., Fanti, G., Flamini, E., Gaborit, V., Grard, R.,  
366 Hamelin, M., Harri, A. M., Hathi, B., Jernej, I., Leese, M. R., Lehto, A., Stoppato, P. F. L., López-Moreno, J. J., Mäkinen,  
367 T., McDonnell, J. A. M., McKay, C. P., Molina-Cuberos, G., Neubauer, F. M., Pirronello, V., Rodrigo, R., Saggin, B.,  
368 Schwingschuh, K., Seiff, A., Simoes, F., Svedhem, H., Tokano, T., Towner, M. C., Trautner, R., Withers, P., Zarnecki,  
369 J. C., 2005. In situ measurements of the physical characteristics of Titan's environment. *Nature* 438, 785–791.
- 370 Gordon, I., Rothman, L., Hill, C., Kochanov, R., Y. Tan, Bernath, P., Birk, M., Boudon, V., Campargue, A., Chance, K.,  
371 Drouin, B., Flaud, J.-M., Gamache, R., Hodges, J., Jacquemart, D., Perevalov, V., Perrin, A., Shine, K., Smith, M.-A.,  
372 Tennyson, J., Toon, G., Tran, H., Tyuterev, V., Barbe, A., Császár, A., Devi, V., Furtenbacher, T., Harrison, J., Hartmann,  
373 J.-M., Jolly, A., Johnson, T., Karman, T., Kleiner, I., Kyuberis, A., Loos, J., Lyulin, O., Massie, S., Mikhailenko, S.,  
374 Moazzen-Ahmadi, N., Müller, H., Naumenko, O., Nikitin, A., Polyansky, O., Rey, M., Rotger, M., Sharpe, S., Sung, K.,  
375 Starikova, E., Tashkun, S., Auwera, J. V., Wagner, G., Wilzewski, J., Wcislo, P., S. Yu, Zak, E., 2017. The HITRAN2012  
376 spectroscopic database. *JQSRT* 203, 3–69.
- 377 Hanel, R., Conrath, B., Flasar, F. M., Kunde, V., Maguire, W., Pearl, J., Pirraglia, J., Samuelson, R., Herath, L., Allison, M.,  
378 Cruikshank, D., Gautier, D., Gierasch, P., Horn, L., Koppany, R., Ponnamperna, C., 1981. Infrared observations of the  
379 Saturnian System from Voyager 1. *Science* 212, 192–200.
- 380 Hébrard, E., Dobrijevic, M., Loison, J. C., Bergeat, A., Hickson, K. M., Caralp, F., 2013. Photochemistry of C<sub>3</sub>H<sub>6</sub> hydrocarbons  
381 in Titan's stratosphere revisited. *Astronomy and Astrophysics* 552.
- 382 Hegelund, F., Andresen, A., Koivisaari, M., 1993. A high resolution infrared study of the  $\nu_9+\nu_{11}-\nu_{11}$ ,  $\nu_{10}+\nu_{11}-\nu_{11}$  hot band  
383 system in allene. *Journal of Molecular Spectroscopy* 159, 230–248.
- 384 Horst, S. M., 2017. Titan's atmosphere and climate. *JGR:Planets* 122 (3), 432–482.

- Hourdin, F., Lebonnois, S., Luz, D., Rannou, P., 2004. Titan's stratospheric composition driven by condensation and dynamics. *Journal of Geophysical Research: Planets* 109, E12005–E12020.
- Irwin, P., Teanby, N., de Kok, R., Fletcher, L., Howett, C., Tsang, C., Wilson, C., Calcutt, S., Nixon, C., Parrish, P., 2008. The NEMESIS planetary atmosphere radiative transfer and retrieval tool. *Journal of Quantitative Spectroscopy and Radiative Transfer* 109, 1136–1150.
- Izon, G., Zerkle, A. L., Williford, K. H., Farquhar, J., Poulton, S. W., Claire, M. W., mar 2017. Biological regulation of atmospheric chemistry en route to planetary oxygenation. *Proceedings of the National Academy of Sciences* 114 (13), E2571–E2579.
- Jacquinet-Husson, N., Armante, R., Scott, N., Chédin, A., Crepeau, L., Boutammine, C., Bouhdaoui, A., Crevoisier, C., Capelle, V., Boone, C., Poulet-Crovisier, N., Barbe, A., Benner, D. C., Boudon, V., Brown, L., Buldyreva, J., Campargue, A., Coudert, L., Devi, V., Down, M., Drouin, B., Fayt, A., Fittschen, C., Flaud, J.-M., Gamache, R., Harrison, J., Hill, C., Hodnebrog, O., Hu, S.-M., Jacquemart, D., Jolly, A., Jimenez, E., Lavrentieva, N., Liu, A.-W., Lodi, L., Lyulin, O., Massie, S., Mikhailenko, S., Muller, H., Naumenko, O., Nikitin, A., Nielsen, C., Orphal, J., Perevalov, V., Perrin, A., Polovtseva, E., Predoi-Cross, A., Rotger, M., Ruth, A., Yu, S., Sung, K., Tashkun, S., Tennyson, J., Tyuterev, V., Auwera, J. V., Voronin, B., Makie, A., 2016. The 2015 edition of the GEISA spectroscopic database. *Journal of Molecular Spectroscopy* 327, 31 – 72.
- Jennings, D. E., Anderson, C. M., Samuelson, R. E., Flasar, F. M., Nixon, C. A., Kunde, V. G., Achterberg, R. K., Cottini, V., de Kok, R., Coustenis, A., Vinatier, S., Calcutt, S. B., 2012. Seasonal disappearance of far-infrared haze in Titan's stratosphere. *The Astrophysical Journal Letters* 754, L3 – L7.
- Jennings, D. E., Flasar, F. M., Kunde, V. G., Nixon, C. A., Segura, M. E., Romani, P. N., Gorius, N., Albright, S., Brasunas, J. C., Carlson, R. C., Mamoutkine, A. A., Guandique, E., Kaelberer, M. S., Aslam, S., Achterberg, R. K., Bjoraker, G. L., Anderson, C. M., Cottini, V., Pearl, J. C., Smith, M. D., Hesman, B. E., Barney, R. D., Calcutt, S., Vellacott, T. J., Spilker, L. J., Edgington, S. G., Brooks, S. M., Ade, P., Schinder, P. J., Coustenis, A., Courtin, R., Michel, G., Fettig, R., Pilorz, S., Ferrari, C., 2017. Composite infrared spectrometer (CIRS) on Cassini. *Applied Optics* 56 (18), 5274 – 5294.
- Jolly, A., Benilan, Y., Manceron, L., Kwabia-Tchana, F., Nixon, C., 2015. Search for evidence of allene on Titan with new spectroscopic data. In: *EPSC Abstracts*. Vol. 10. pp. EPSC2015–171.
- Jolly, A., Fayt, A., Benilan, Y., Jacquemart, D., Nixon, C. A., Jennings, D. E., 2010. The  $\nu_8$  bending mode of diacetylene: from laboratory spectroscopy to the detection of  $^{13}\text{C}$  isotopologues in Titan's atmosphere. *The Astrophysical Journal* 714, 852–859.
- Koga, Y., Kondo, S., Nakanagaand, T., Saeki, S., 1979. Infrared absorption intensities of allene. *Journal of Chemical Physics* 71, 2404–2411.
- Krasnopolsky, V. A., 2014. Chemical composition of titan's atmosphere and ionosphere: Observations and the photochemical model. *Icarus* 236, 83–91.
- Lacis, A., Oinas, V., 1991. A description of the correlated k distribution method for modeling nongray gaseous absorption, thermal emission, and multiple scattering in vertically inhomogeneous atmospheres. *Journal of Geophysical Research* 96, 9027–9063.
- Lebonnois, S., Toubanc, D., Hourdin, F., Rannou, P., 2001. Seasonal variations of Titan's atmospheric composition. *Icarus* 152, 384–406.
- Lellouch, E., Bézard, B., Flasar, F., Vinatier, S., Achterberg, R., Nixon, C., Bjoraker, G., Gorius, N., 2014. The distribution of methane in Titan's stratosphere from Cassini/CIRS observations. *Icarus* 231, 323 – 337.
- Li, C., Zhang, X., Gao, P., Yung, Y., 2015. Vertical distribution of  $\text{C}_3$  hydrocarbons in Titan's atmosphere. *The Astrophysical Journal Letters* 803, L19 – L26.
- Loison, J., Hébrard, E., Dobrijevic, M., Hickson, K., Caralp, F., Hue, V., Gronoff, G., Venot, O., Bénilan, Y., 2015. The neutral photochemistry of nitriles, amines and imines in the atmosphere of titan. *Icarus* 247, 218–247.
- Magee, B. A., Waite, J. H., Mandt, K. E., Westlake, J., Bell, J., Gell, D. A., 2009. INMS-derived composition of Titan's upper atmosphere: Analysis methods and model comparison. *Planetary and Space Science* 57, 1895–1916.
- Maguire, W. C., Hanel, R. A., Jennings, D. E., Kunde, V. G., Samuelson, R. E., 1981.  $\text{C}_3\text{H}_8$  and  $\text{C}_3\text{H}_4$  in Titan's atmosphere. *Nature* 292, 683–686.
- Müller-Woodarg, I., Griffith, C. A., Lellouch, E., Cravens, T. E. (Eds.), 2014. *Titan Interior, Surface, and Space Environment*. Cambridge University Press.
- Niemann, H. B., Atreya, S. K., Demick, J. E., Gautier, D., Haberman, J. A., Harpold, D. N., Kasprzak, W. T., Lunine, J. I., Owen, T. C., Raulin, F., 2010. Composition of titan's lower atmosphere and simple surface volatiles as measured by the Cassini/Huygens probe gas chromatograph mass spectrometer experiment. *Journal of Geophysical Research* 115, E12006–E12028.
- Nixon, C., Achterberg, R., Teanby, N., Irwin, P., Flaud, J.-M., Kleiner, I., Dehayem-Kamadjeu, A., Brown, L., Sams, R., Bézard, B., Coustenis, A., Ansty, T., Mamoutkine, A., Vinatier, S., Bjoraker, G., Jennings, D., Romani, P., Flasar, F. M., 2010. Upper limits for undetected trace species in the stratosphere of Titan. *Faraday Discussions* 147, 95.
- Nixon, C., Jennings, D., Flaud, J.-M., Bézard, B., Teanby, N., Irwin, P., Ansty, T., Coustenis, A., Vinatier, S., Flasar, F., 2009. Titan's prolific propane: A Cassini CIRS perspective. *Planetary and Space Science* 57, 1573–1585.
- Nixon, C. A., Jennings, D. E., Bézard, B., Vinatier, S., Teanby, N. A., Sung, K., Ansty, T. M., Irwin, P. G. J., Gorius, N., Cottini, V., Coustenis, A., Flasar, F. M., 2013. Detection of propene in Titan's atmosphere. *The Astrophysical Journal Letters* 776, L14 – L20.
- Roe, H. G., Greathouse, T., Tokunaga, A., 2011. Update on the TEXES Titan mid-infrared spectral survey. In: *EPSC-DPS Joint Meeting 2011*. p. 1398.
- Sung, K., Toon, G. C., Drouin, B. J., Mantz, A. W., Smith, M. A. H., 2018. FT-IR measurements of cold propene ( $\text{C}_3\text{H}_6$ )

450 cross-sections at temperatures between 150 and 299K. *Journal of Quantitative Spectroscopy and Radiative Transfer* 213,  
451 119–132.

452 Sung, K., Toon, G. C., Mantz, A. W., Smith, M. A. H., 2013. FT-IR measurements of cold C<sub>3</sub>H<sub>8</sub> cross sections at 7-15 microns  
453 for Titan atmosphere. *Icarus* 226.

454 Teanby, N., de Kok, R., Irwin, P., 2009a. Small-scale composition and haze layering in titan’s polar vortex. *Icarus* 204 (2),  
455 645–657.

456 Teanby, N., Irwin, P., de Kok, R., Jolly, A., Bézard, B., Nixon, C., Calcutt, S., 2009b. Titan’s stratospheric C<sub>2</sub>N<sub>2</sub>, C<sub>3</sub>H<sub>4</sub>, and  
457 C<sub>4</sub>H<sub>2</sub> abundances from Cassini/CIRS far-infrared spectra. *Icarus* 202, 620–631.

458 Teanby, N., Irwin, P., de Kok, R., Vinatier, S., Bézard, B., Nixon, C., Flasar, F., Calcutt, S., Bowles, N., Fletcher, L., Howett,  
459 C., Taylor, F., 2007. Vertical profiles of HCN, HC<sub>3</sub>N, and C<sub>2</sub>H<sub>2</sub> in Titan’s atmosphere derived from Cassini/CIRS data.  
460 *Icarus* 186, 364–384.

461 Teanby, N. A., Patrick G. J. Irwin and, C. A. N., de Kok, R., Vinatier, S., Coustenis, A., Sefton-Nash, E., Calcutt, S. B.,  
462 Flasar, F. M., 2012. Active upper-atmosphere chemistry and dynamics from polar circulation reversal on Titan. *Nature* 491,  
463 732–735.

464 Trainer, M. G., Sebree, J. A., Yoon, Y. H., Tolbert, M. A., 2013. THE INFLUENCE OF BENZENE AS a TRACE REACTANT  
465 IN TITAN AEROSOL ANALOGS. *The Astrophysical Journal* 766 (1), L4–L9.

466 Vinatier, S., Bézard, B., Fouchet, T., Teanby, N., de Kok, R., Irwin, P. G. J., Conrath, B. J., Romani, P. N., Flasar, F. M.,  
467 Coustenis, A., 2007. Vertical abundance profiles of hydrocarbons in Titan’s atmosphere at 15S and 80N retrieved from  
468 Cassini/CIRS spectra. *Icarus* 188, 120–138.

469 Vinatier, S., Bézard, B., Lebonnois, S., Teanby, N. A., Achterberg, R. K., Gorius, N., Mamoutkine, A., Guandique, E., Jolly,  
470 A., Jennings, D. E., Flasar, F. M., 2015. Seasonal variations in Titan’s middle atmosphere during the northern spring derived  
471 from Cassini / CIRS observations. *Icarus* 250, 95–115.

472 Wilson, E. H., Atreya, S. K., 2004. Current state of modeling the photochemistry of Titan’s mutually dependent atmosphere  
473 and ionosphere. *Journal of Geophysical Research* 109.

474 Yung, Y. L., Allen, M., Pinto, J. P., 1984. Photochemistry of the atmosphere of Titan: Comparison between model and  
475 observations. *The Astrophysical Journal Supplement Series* 55, 465–506.

FP3													
		2004-2009			2012-2015								
		20°S-20°N			20°S-20°N			20°N-60°N					
		0°N			1°N			34°N					
Avg Lat		60°S-20°S			60°S-20°S			20°N-60°N					
		42°S			60°S-20°S			34°N					
Altitude (km)		spectra	NESR	spectra	NESR	spectra	NESR	spectra	NESR	spectra	NESR		
100-150		322	1.58	330	1.68	412	1.53	299	2.30	440	1.82	288	2.41
150-200		451	1.37	428	1.48	537	1.37	416	1.96	608	1.67	395	2.19
200-250		515	1.32	460	1.50	568	1.30	441	1.85	601	1.61	464	1.89
250-300		496	1.34	440	1.45	634	1.23	463	1.99	680	1.60	446	1.74
300-350		271	1.67	299	1.79	294	1.60	229	2.60	297	2.16	341	1.92
350-375		235	1.96	242	1.89	258	1.59	218	2.33	287	2.21	191	2.70

FP4													
Altitude (km)		spectra	NESR	spectra	NESR	spectra	NESR	spectra	NESR	spectra	NESR		
100-150		310	0.29	369	0.23	515	0.29	388	0.40	345	0.30	298	0.33
150-200		381	0.22	463	0.27	652	0.23	530	0.27	488	0.30	397	0.32
200-250		372	0.24	573	0.24	691	0.17	551	0.21	503	0.26	464	0.29
250-300		334	0.26	559	0.19	728	0.18	583	0.20	556	0.23	450	0.24
300-350		187	0.39	450	0.22	345	0.28	305	0.29	230	0.33	336	0.28
350-400		187	0.29	277	0.30	294	0.30	265	0.32	232	0.38	183	0.29

Table 1: Observations averaged. Listed are the middle altitude, number of spectra averaged, and the noise equivalent spectral radiance (NESR) for each altitude bin. NESRs have units of  $\text{nW cm}^{-2} \text{sr}^{-1} \text{cm}$ , and were derived from the standard deviation of the mean for each average, and were measured at  $910 \text{ cm}^{-1}$  for FP3, and  $1280 \text{ cm}^{-1}$  for FP4.

476 **List of Figures**

477 1 Distribution of all Mid-IR Limb Integrations (MIRLMBINT) observations during the Cassini  
478 mission shown as black circles. Temperatures are shown as contours (colored) and correspond  
479 to those at 1 mbar, or about 175 km, and are updated from Achterberg et al. (2014). The  
480 black boxes indicate the binning scheme with two time spans (2004-2009 and 2012-2015)  
481 further binned to three latitude ranges (60°S-20°S, 20°S-20°N, and 20°N-60°N). The dashed  
482 black line surrounded by gray is the solar latitude of Titan, where the Sun is directly overhead  
483 at 1200 local time. . . . . 17  
484 2 Spectra used in the 2004-2009 equatorial temperature retrieval of the methane  $\nu_4$  band. The  
485 altitude label corresponds to the peak contribution altitude, see Fig. 3 . . . . . 18  
486 3 Normalized temperature contribution functions for each altitude bin, taken at  $1311\text{ cm}^{-1}$ .  
487 Altitude bins are listed immediately to the right of each contribution function. The altitude  
488 where the contribution function peaks is listed in parantheses. In most cases, altitudes of  
489 peak contribution are not the center altitude for each bin. . . . . 19  
490 4 Comparison of retrieved temperatures in the 2012-2015 time span.  $1-\sigma$  error bars are given  
491 at altitudes where the contribution function peaks in each altitude bin. The solid gray line is  
492 the a priori profile with error envelope. Dot dashed lines are the retrieved profile where there  
493 are no spectra. . . . . 20  
494 5 Normalized propene contribution functions for each altitude bin, taken at  $912.5\text{ cm}^{-1}$ . Al-  
495 titude bins are listed immediately to the right of each contribution function. The altitude  
496 where the contribution function peaks is listed in parantheses. In most cases, altitudes of  
497 peak contribution are not the center altitude for each bin. . . . . 21  
498 6 Spectral fits for propene and propane for the 2004-2009 time span in the equatorial bin. . . . 22  
499 7 Spectral fits used in the 2004-2009 south propyne retrieval. . . . . 23  
500 8 Vertical profiles  $\text{C}_3\text{H}_4$ (top),  $\text{C}_3\text{H}_6$  (middle),  $\text{C}_3\text{H}_8$  (bottom). Black is the northern bin, blue  
501 is the equatorial bin, and green is the southern bin. Volume mixing ratios are given as solid  
502 lines.  $1-\sigma$  errors are given as colored regions, dot-dashed lines, or horizontal error bars at  
503 altitudes of peak contribution. . . . . 24  
504 9 Vertical profiles of our retrieved gases. Volume mixing ratios for the 2004-2009 time span are  
505 solid lines and volume mixing ratios for the 2012-2015 time span are dotted lines.  $1-\sigma$  errors  
506 are given as errorbars at peak contribution altitudes. . . . . 25  
507 10 Our 2004-2009 20°S - 20°N profile compared with published predictions for propene's abun-  
508 dance. Errors on Hebrard 2013 correspond to 75th percentile, Loison 2015 correspond to 90th  
509 percentile, Dobrijevic 2016 correspond to 90th percentile. Nixon 2013 values are inferred  
510 abundances and uncertainties described in Nixon et al. (2013). Of the models compared, only  
511 Loison 2015 has a similar shape and abundance to our measured values. . . . . 26  
512 11 Comparison of modeled spectrum without allene (green) and forward modeled spectrum in-  
513 cluding allene (blue), against the observed spectrum (black). Differences in the spectra are  
514 most easily noted in the residuals, where contributions from allene are seen as peaks in the  
515 dashed spectrum, noted by asterisks. . . . . 27  
516 12 Plot of the  $\Delta\chi^2$  against allene abundance.  $\Delta\chi^2$  is calculated by subtracting the  $\chi^2$  calculated  
517 from the forward model with allene included in the atmosphere from the  $\chi^2$  value calculated  
518 from retrieved spectrum that does not include allene. Along these lines, a negative  $\Delta\chi^2$   
519 indicates the model-fit has improved, whereas a positive value indicates the fit is worsened.  
520 The minimum value is around -4.5 near  $1 \times 10^{-9}$ , leading us to an estimated  $2-\sigma$  upper limit  
521 of 1 ppbv. . . . . 28

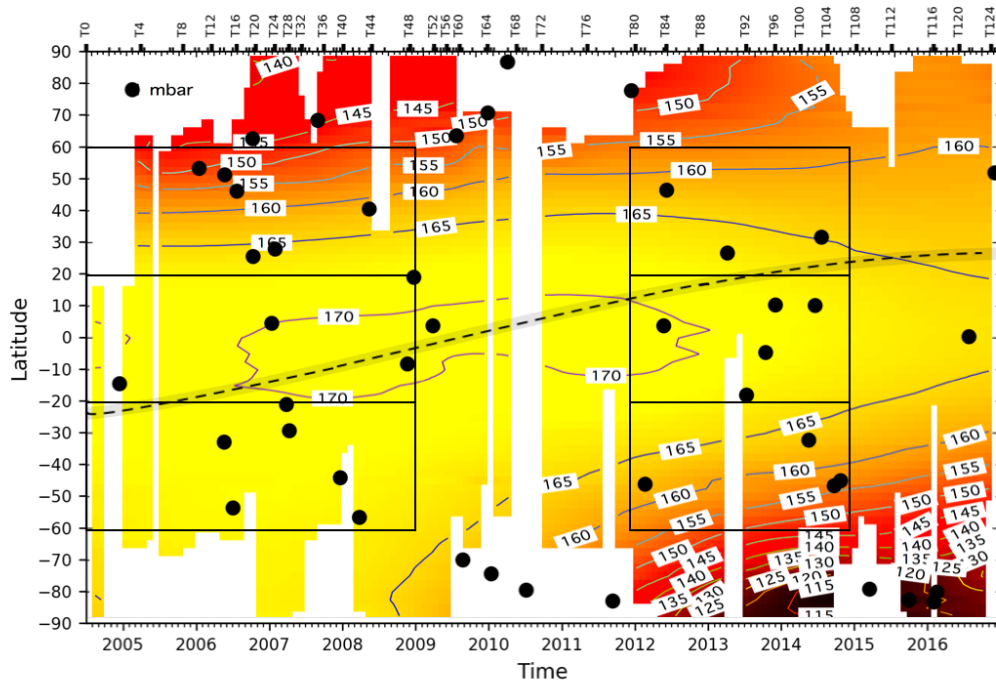


Figure 1: Distribution of all Mid-IR Limb Integrations (MIRLBINT) observations during the Cassini mission shown as black circles. Temperatures are shown as contours (colored) and correspond to those at 1 mbar, or about 175 km, and are updated from Achterberg et al. (2014). The black boxes indicate the binning scheme with two time spans (2004-2009 and 2012-2015) further binned to three latitude ranges ( $60^{\circ}\text{S}$ - $20^{\circ}\text{S}$ ,  $20^{\circ}\text{S}$ - $20^{\circ}\text{N}$ , and  $20^{\circ}\text{N}$ - $60^{\circ}\text{N}$ ). The dashed black line surrounded by gray is the solar latitude of Titan, where the Sun is directly overhead at 1200 local time.

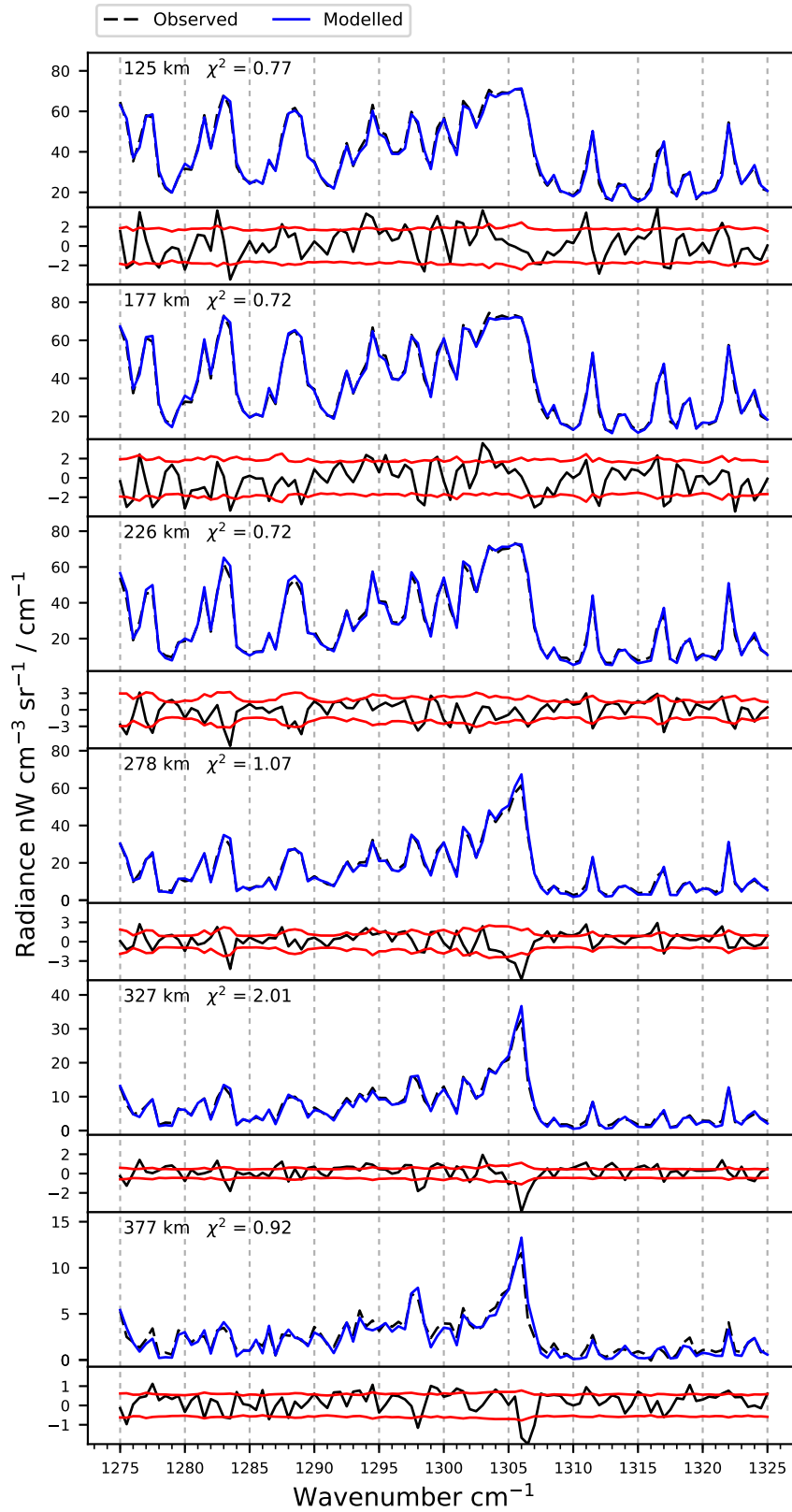


Figure 2: Spectra used in the 2004-2009 equatorial temperature retrieval of the methane  $\nu_4$  band. The altitude label corresponds to the peak contribution altitude, see Fig. 3

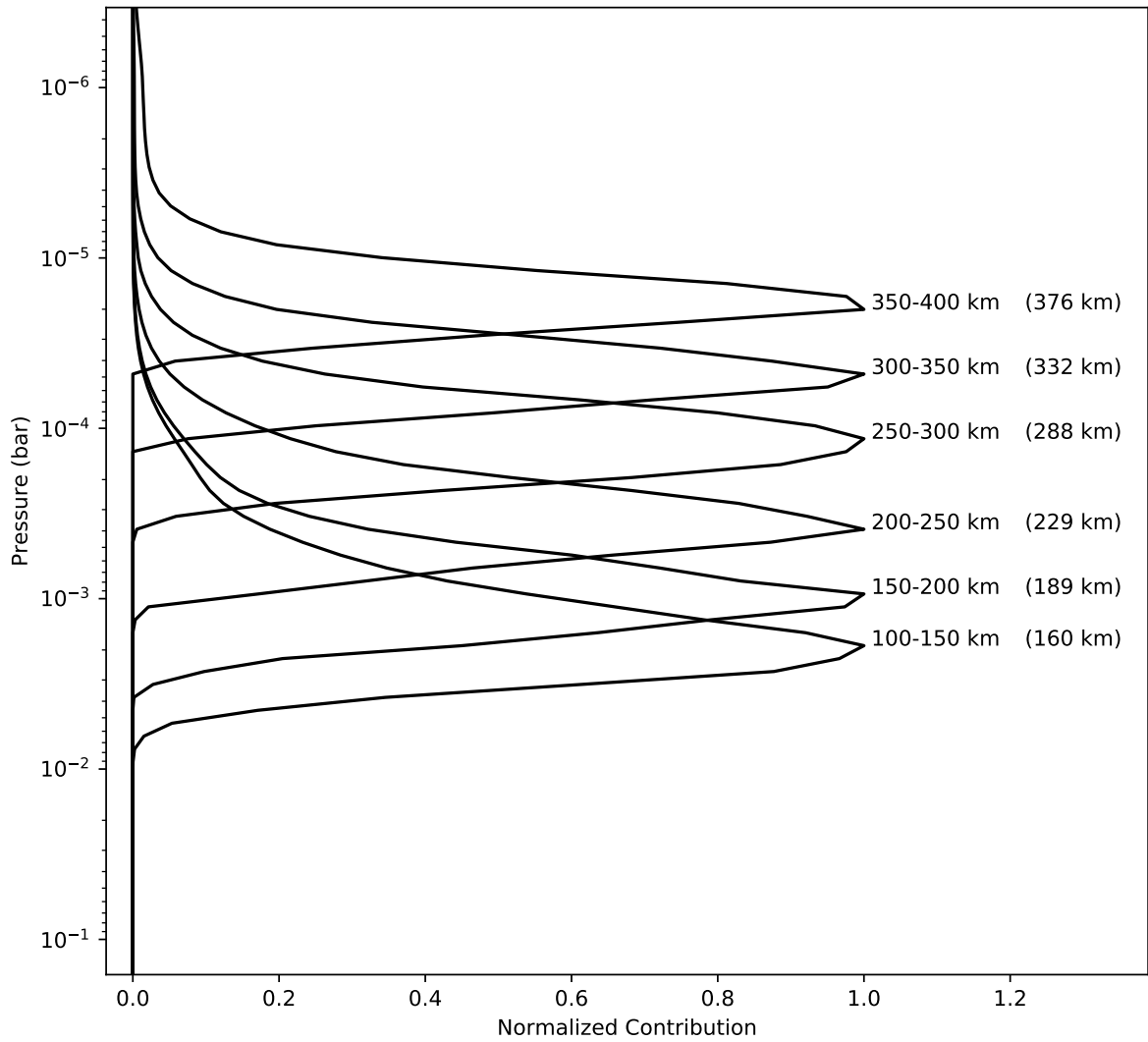


Figure 3: Normalized temperature contribution functions for each altitude bin, taken at  $1311 \text{ cm}^{-1}$ . Altitude bins are listed immediately to the right of each contribution function. The altitude where the contribution function peaks is listed in parentheses. In most cases, altitudes of peak contribution are not the center altitude for each bin.

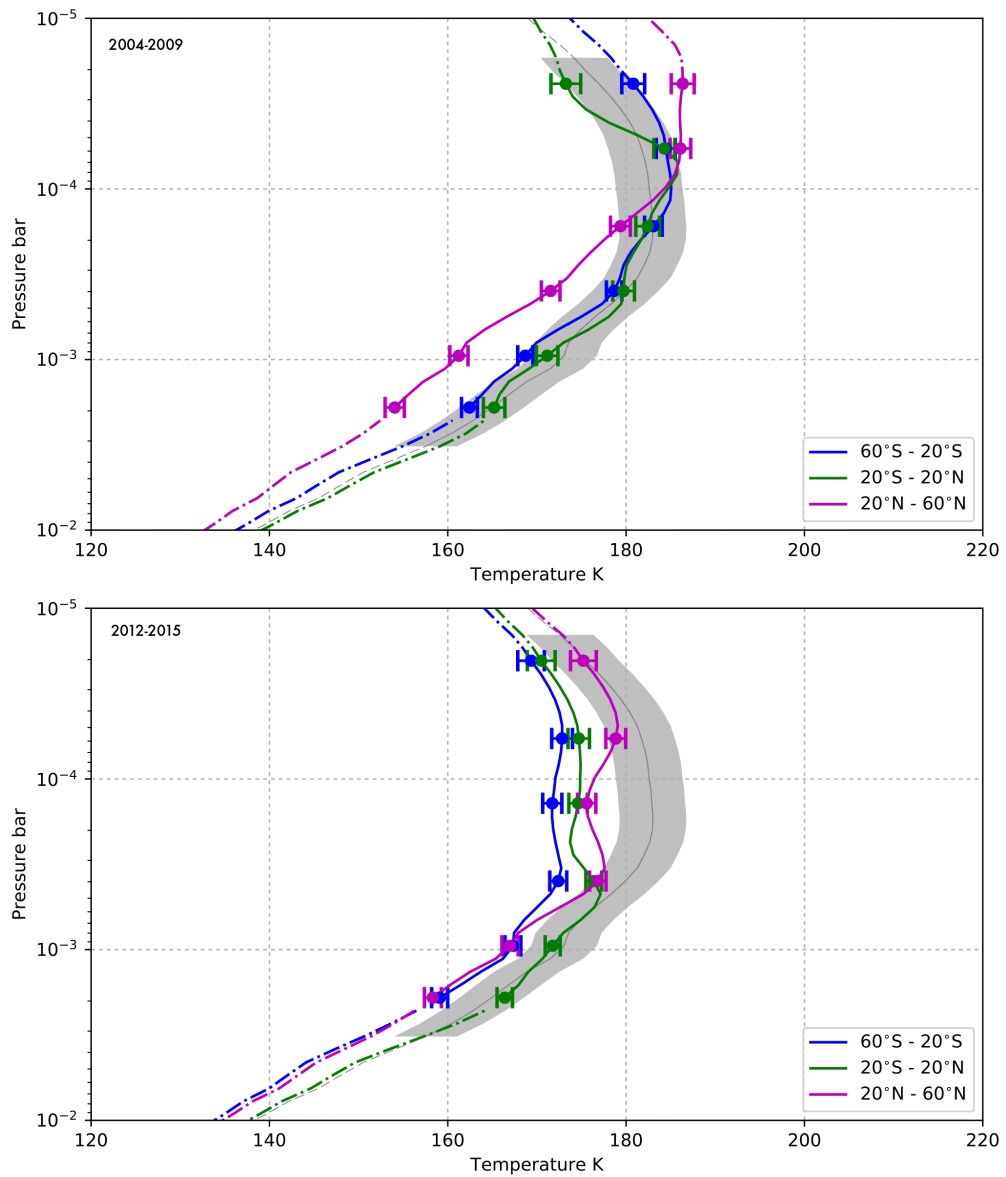


Figure 4: Comparison of retrieved temperatures in the 2012-2015 time span.  $1-\sigma$  error bars are given at altitudes where the contribution function peaks in each altitude bin. The solid gray line is the a priori profile with error envelope. Dot dashed lines are the retrieved profile where there are no spectra.

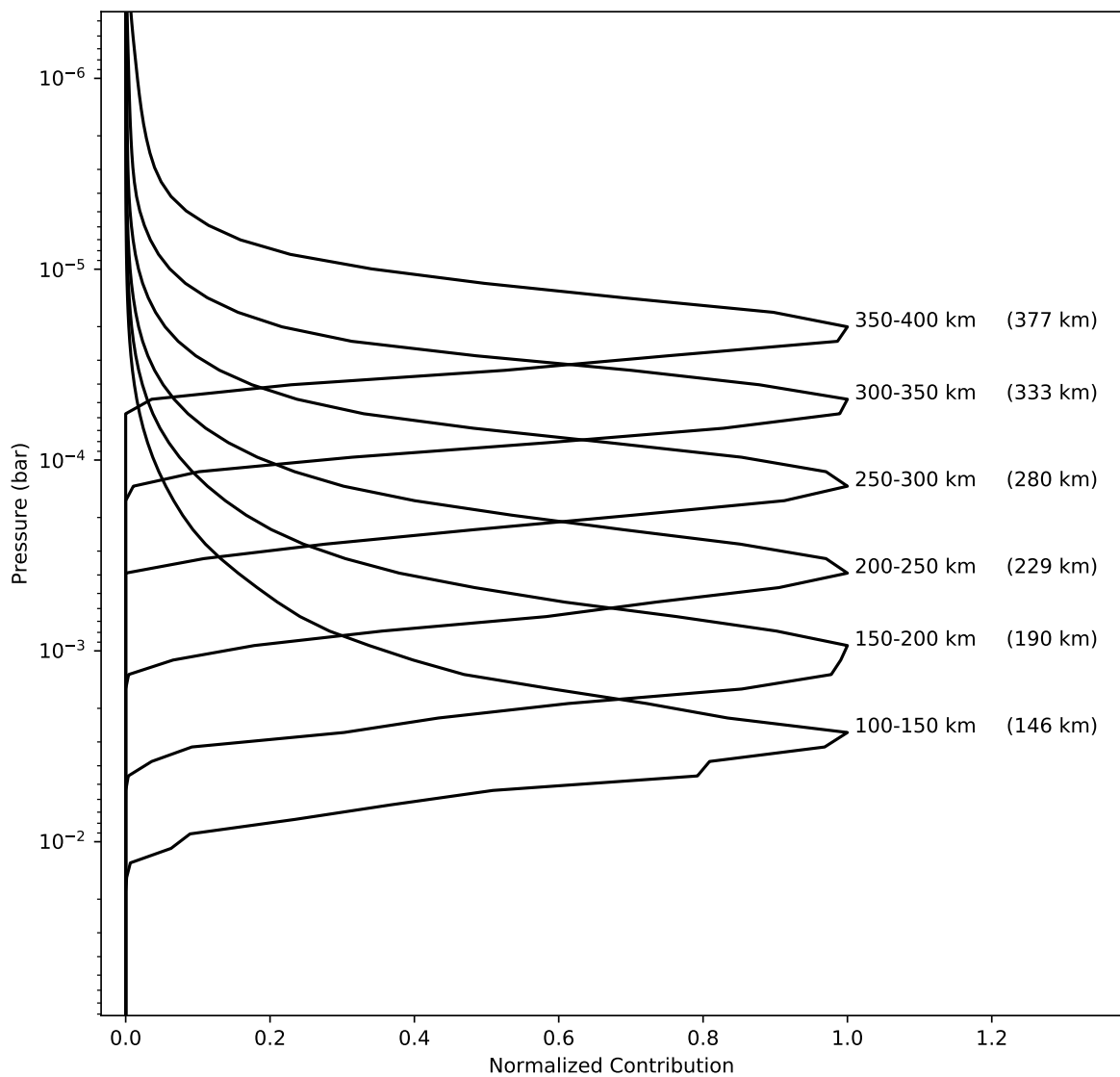


Figure 5: Normalized propene contribution functions for each altitude bin, taken at  $912.5 \text{ cm}^{-1}$ . Altitude bins are listed immediately to the right of each contribution function. The altitude where the contribution function peaks is listed in parentheses. In most cases, altitudes of peak contribution are not the center altitude for each bin.

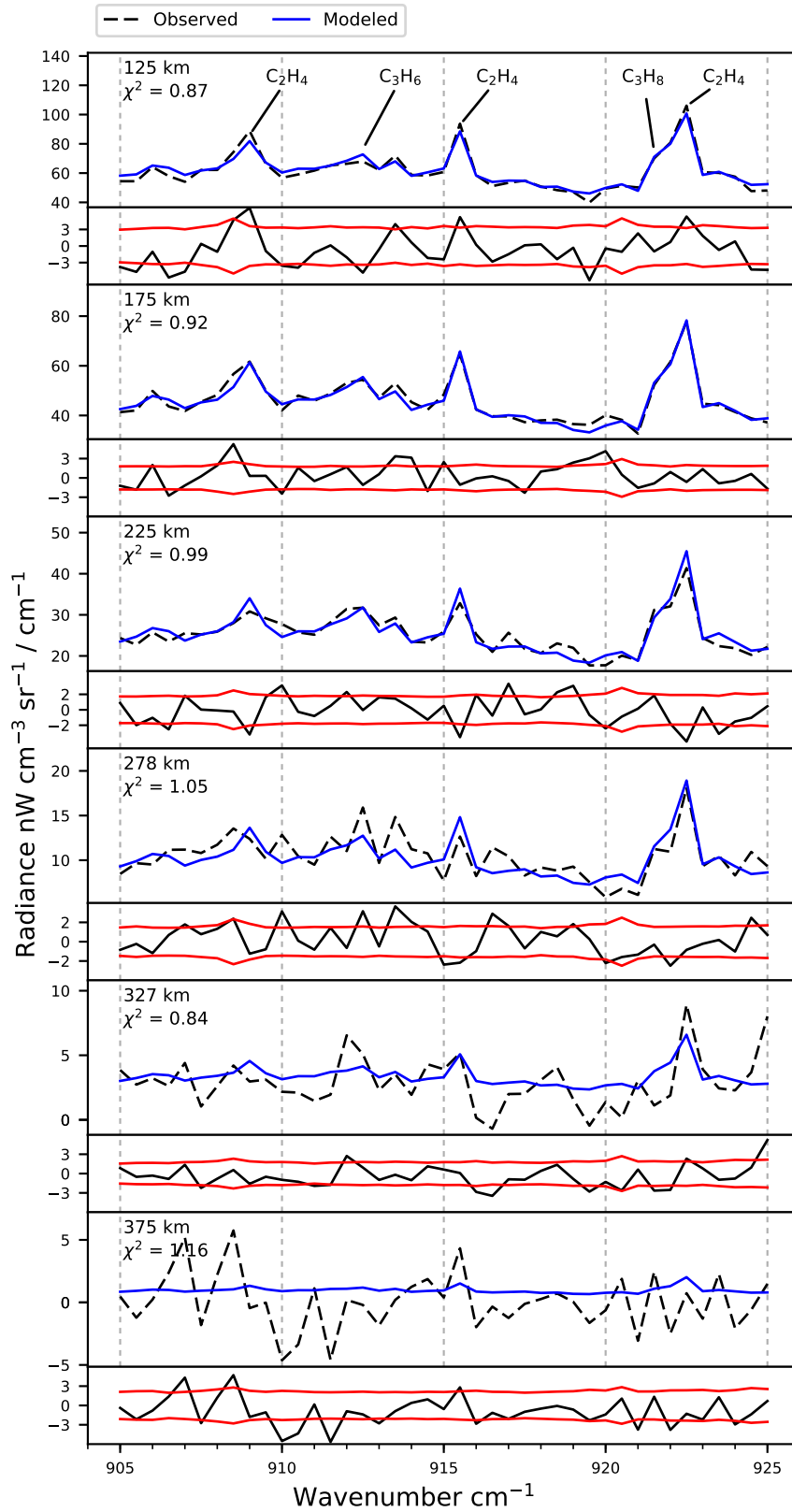


Figure 6: Spectral fits for propene and propane for the 2004-2009 time span in the equatorial bin.

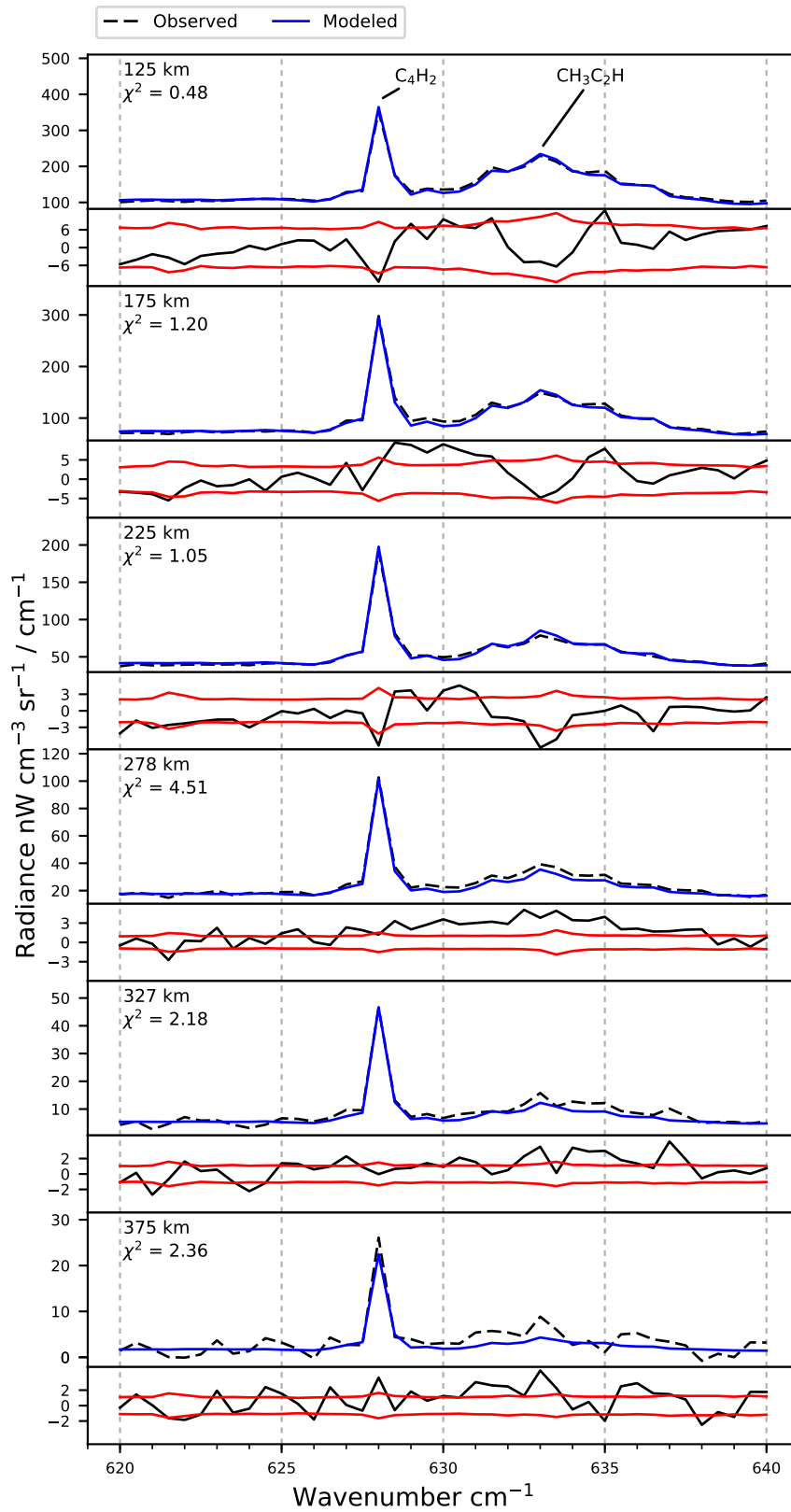


Figure 7: Spectral fits used in the 2004-2009 south propyne retrieval.

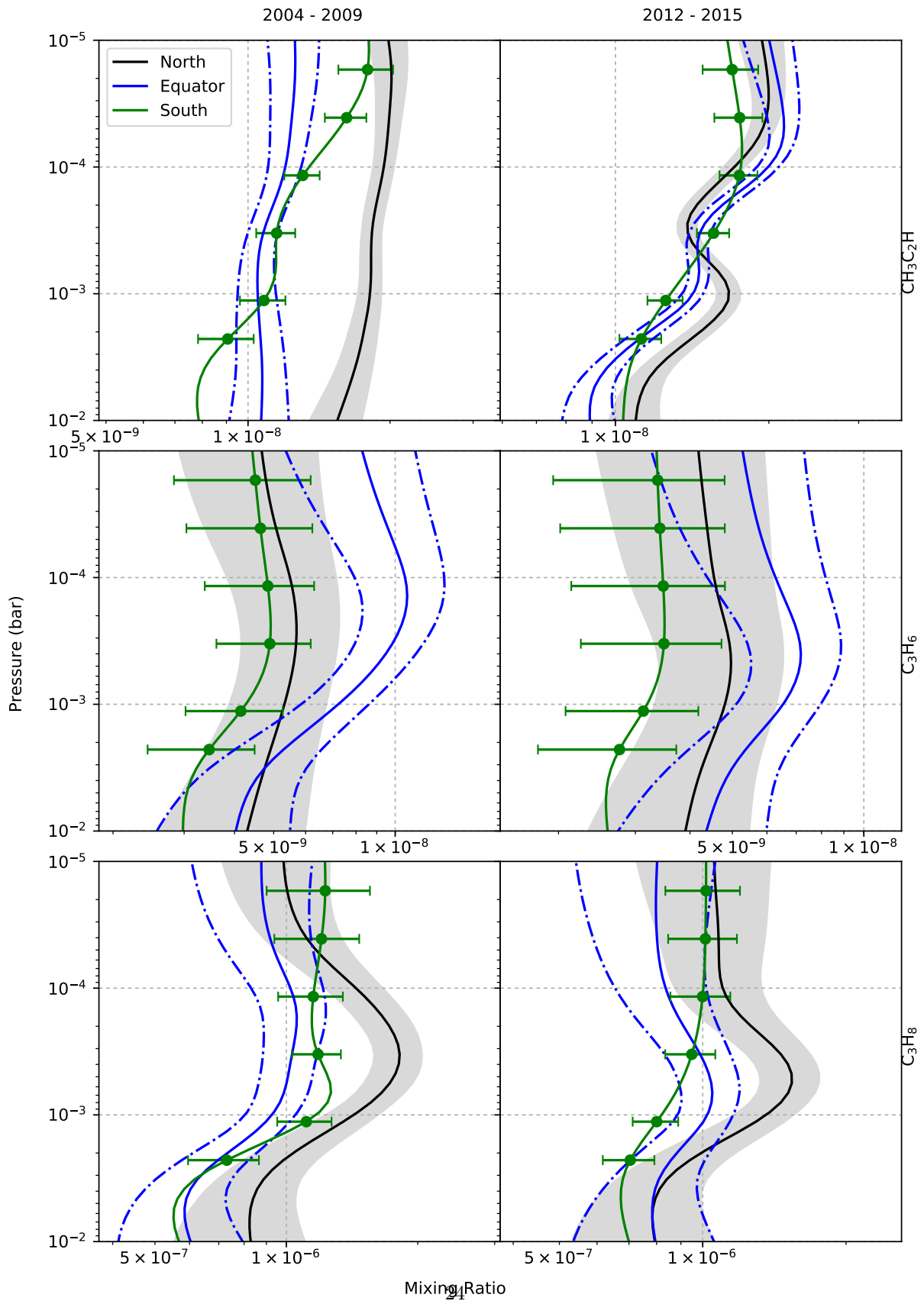


Figure 8: Vertical profiles  $C_3H_4$  (top),  $C_3H_6$  (middle),  $C_3H_8$  (bottom). Black is the northern bin, blue is the equatorial bin, and green is the southern bin. Volume mixing ratios are given as solid lines.  $1-\sigma$  errors are given as colored regions, dot-dashed lines, or horizontal error bars at altitudes of peak contribution.

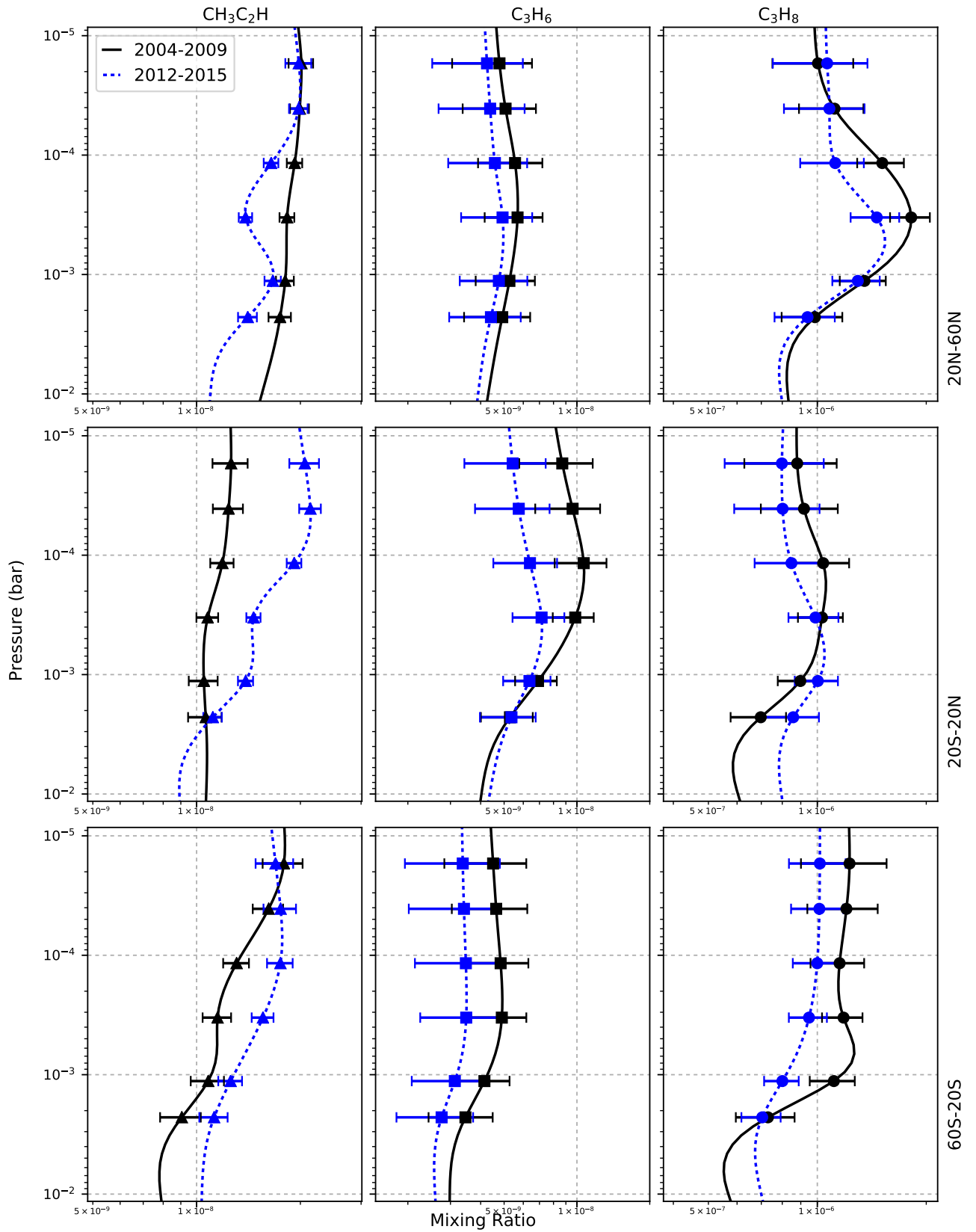


Figure 9: Vertical profiles of our retrieved gases. Volume mixing ratios for the 2004-2009 time span are solid lines and volume mixing ratios for the 2012-2015 time span are dotted lines.  $1-\sigma$  errors are given as errorbars at peak contribution altitudes.

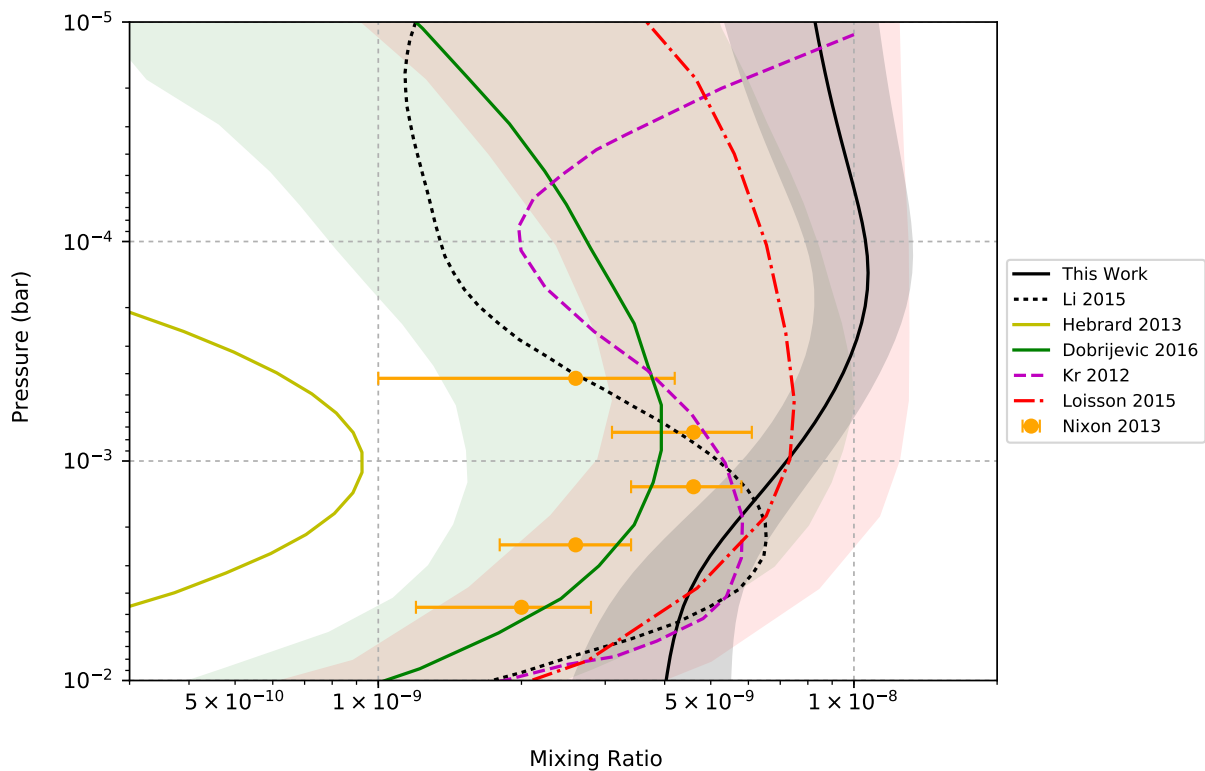


Figure 10: Our 2004-2009 20°S - 20°N profile compared with published predictions for propene's abundance. Errors on Hebrard 2013 correspond to 75th percentile, Loisson 2015 correspond to 90th percentile, Dobrijevic 2016 correspond to 90th percentile. Nixon 2013 values are inferred abundances and uncertainties described in Nixon et al. (2013). Of the models compared, only Loisson 2015 has a similar shape and abundance to our measured values.

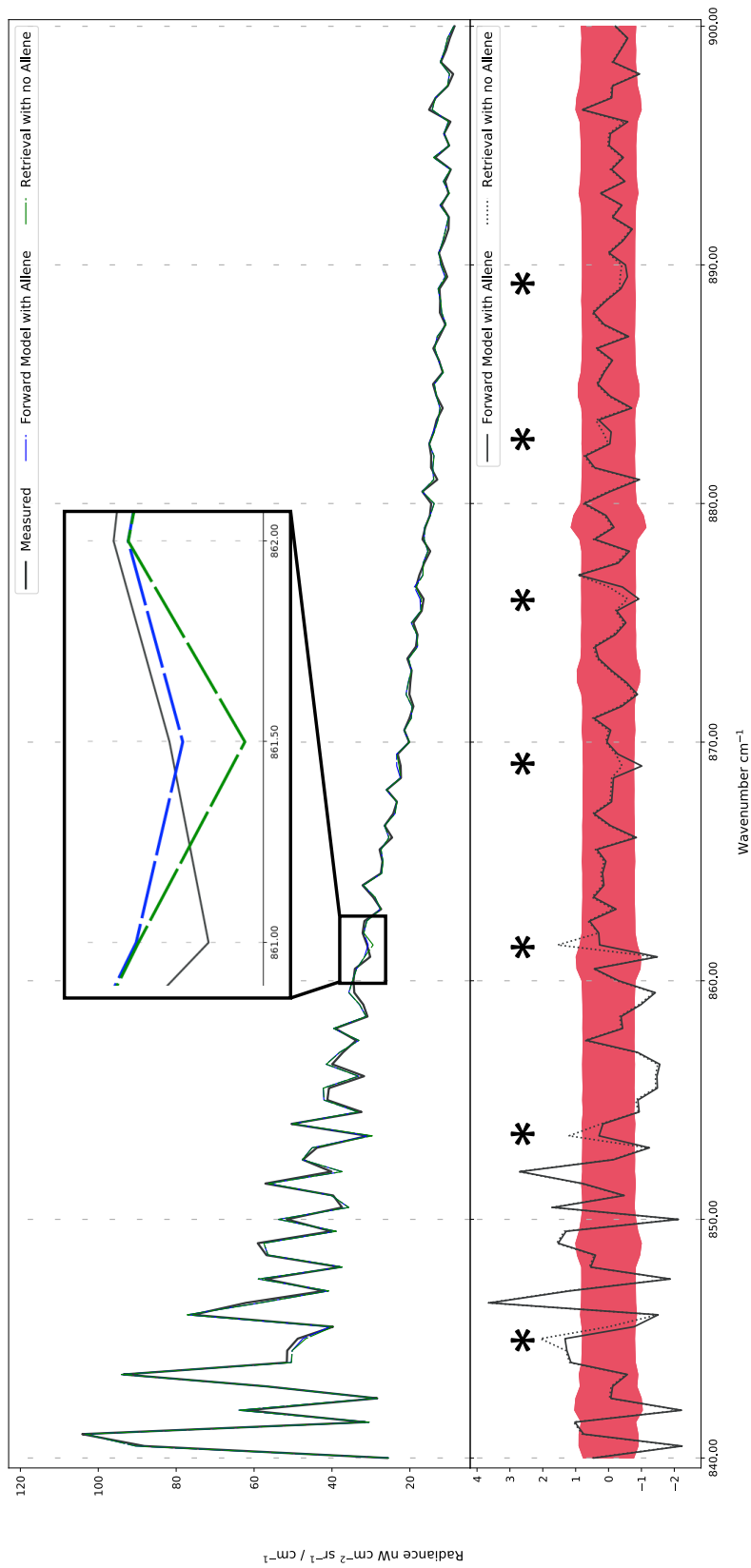


Figure 11: Comparison of modeled spectrum without allene (green) and forward modeled spectrum including allene (blue), against the observed spectrum (black). Differences in the spectra are most easily noted in the residuals, where contributions from allene are seen as peaks in the dashed spectrum, noted by asterisks.

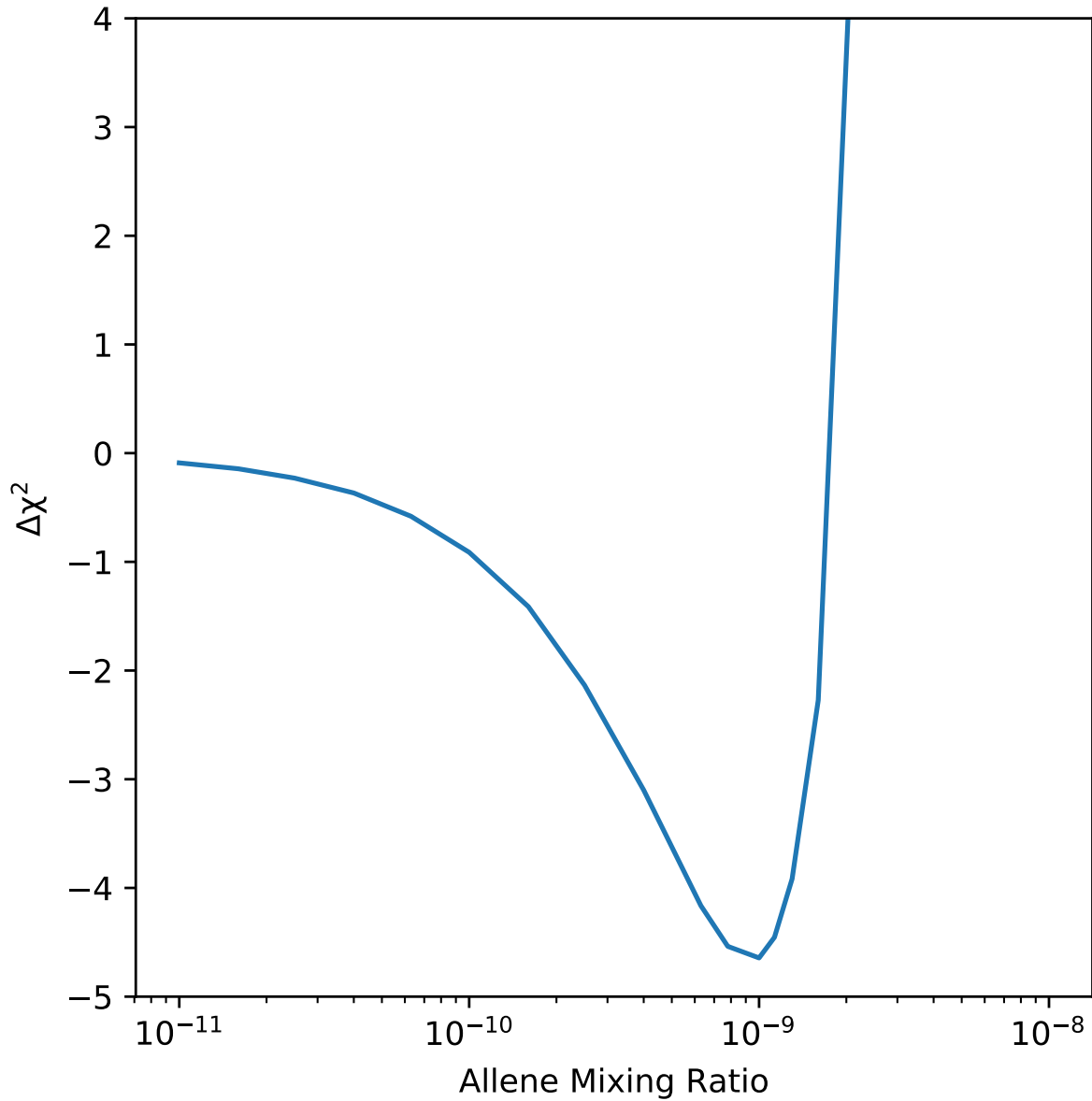


Figure 12: Plot of the  $\Delta\chi^2$  against allene abundance.  $\Delta\chi^2$  is calculated by subtracting the  $\chi^2$  calculated from the forward model with allene included in the atmosphere from the  $\chi^2$  value calculated from retrieved spectrum that does not include allene. Along these lines, a negative  $\Delta\chi^2$  indicates the model-fit has improved, whereas a positive value indicates the fit is worsened. The minimum value is around -4.5 near  $1 \times 10^{-9}$ , leading us to an estimated  $2\text{-}\sigma$  upper limit of 1 ppbv.